IEEE Sensors Letters VOL. 7, NO. 9, SEPTEMBER 2023

Dual Localized Surface Plasmon Resonance Sensors on a Single Optical Fiber

Nafize I. Hossain[1,2], SK Nayemuzzaman[1,3], and Shawana Tabassum[1,*]

[1] *Department of Electrical Engineering, The University of Texas at Tyler, Tyler, TX 75799, USA*
[2] *Department of Electrical and Computer Engineering, Tufts University, Medford, MA 02155, USA*
[3] *Department of Electrical and Computer Engineering, The University of Texas at Dallas, Richardson, TX 75080, USA*
** Member, IEEE*

Received 1 Nov 2016, revised 25 Nov 2016, accepted 30 Nov 2016, published 5 Dec 2016, current version 15 Dec 2016. (Dates will be inserted by IEEE; "published" is the date the accepted preprint is posted on IEEE Xplore®; "current version" is the date the typeset version is posted on Xplore®).

Abstract—This letter reports a novel dual sensor based on localized surface plasmon resonance near the tip of an optical fiber. The sensor was fabricated by immobilizing two regions of the fiber with gold nanoparticles of different sizes. The evanescent field of the incident light interacted with the metal nanoparticles at the fiber tip and produced localized surface plasmon resonance at two distinct wavelengths. This multiplexing capability of a single fiber allows the detection of multiple analytes in a smaller footprint, reducing the number of fibers required for multi-analyte sensing. The dual-coated fiber demonstrated localized surface plasmon resonance dips at 610 and 662 nm wavelengths, in contrast to the fiber coated with a single layer of gold nanoparticles which exhibited a resonance dip at 620 nm. The performance of the dual sensor was tested with varying concentrations of ethanol (ranging from 0 to 100%). The resonance dips located at 610 and 662 nm showed variations in reflection intensities when ethanol was adsorbed onto the surface of the gold nanoparticles. Additionally, the sensor performance was analyzed at different temperatures (at 25°C, 40°C, and 60°C) and bending deformations (at 10° up to 30, 60, and 90 cycles). Temperature corrections were incorporated to compensate for variations in the sensor response caused by temperature changes. The sensor showed an excellent reproducible response under bending deformations. The presented design could be extended to implement multiple sensing regions on the same fiber, enabling the detection of multiple analytes with a single optical fiber.

Index Terms—Fiber-optic sensor, gold nanoparticles, localized surface plasmon resonance, dual sensing.

I. INTRODUCTION

In various applications such as biosensing, healthcare, and environmental monitoring, there is a demand for high-throughput spatiotemporal analysis of biomolecules. Traditional spectrophotometric analytical systems, including liquid chromatography/mass spectroscopy, ultraviolet-visible spectroscopy, Fourier transform infrared spectroscopy, and Matrix-assisted laser desorption/ionization spectroscopy, are effective but suffer from high cost, bulkiness, and lack of *in situ* monitoring capabilities [1], [2]. Miniaturized fiber-optic analytical devices offer a potential solution, utilizing light-matter interactions in fluidic environments known as optofluidics [3], [4]. However, current fabrication methods involving micromachining the fibers are expensive and challenging for integration into miniaturized systems [5], [6]. Additionally, existing integrated optofluidic devices using optical fibers often require complex alignment between the fiber and the flow system, resulting in decreased signal yields [7], [8]. There is a need for multiplexed sensing to analyze molecules in a complex medium. Unlike conventional optical fiber-based multiplexed biosensing with bundles of fibers that substantially increase the footprint and number of coupling elements between fibers and free space [9], [10], a fiber-optic sensor that eliminates cleanroom-based fabrication, enables multiplexed monitoring with a single fiber, and offers in situ monitoring capabilities, presents significant potential for sensing applications.

This study presents a dual sensor realized at the distal end of an optical fiber, which was demonstrated to measure various concentrations of an analyte (i.e., ethanol) in deionized water. The fiber-optic sensor features two sensing regions immobilized with gold nanoparticles (AuNPs), exhibiting two distinct localized surface plasmon resonances (LSPR). These LSPR interactions with the analyte produced reflected light intensity proportional to its concentration. We measured intensity variations rather than resonance wavelength shifts since LSPR-based sensors have been shown to exhibit higher sensitivity in the intensity modulation scheme [11]. The fiber-optic sensor was fabricated without relying on cleanroom-based fabrication methods, enabling simplified manufacturing, improved adjustability, and real-time in situ biosensing. Experimental analyses involved varying the temperature of the analyte solution and bending the fiber at a specific angle to evaluate the sensor's performance. The fiber-optic sensor demonstrated excellent reproducibility across different bending cycles (30, 60, and 90), with a coefficient of variance below 2.5%. This simplified and cost-effective fiber-optic sensing platform holds potential for future in situ biosensing in complex environments where simultaneous measurements of multiple analytes are required. The presented dual sensing platform can be easily expanded to a multiplexed design.

Corresponding author: S. Tabassum (stabassum@uttyler.edu).
Digital Object Identifier: 10.1109/LSEN.2023.3300815.

II. MATERIALS AND METHODS

A. Fabrication of the Fiber-tip LSPR Sensor

An approximately 2.5 cm segment located at the tip of a fused silica fiber (2 × 1 multimode fiber coupler, # TT200R5S1B, Thorlabs Inc., Newton, NJ, USA) with a diameter of 200 µm was selected for functionalization with two different sizes of gold nanoparticles (AuNPs). Fig. 1 shows the formation of the dual LSPR sensors on the fiber surface. The process began by removing the cladding from the 2.5 cm-long fiber using acetone (Fig. 1a). Subsequently, the de-cladded fiber section was cleaned and treated with a Piranha solution (a mixture of H_2SO_4 and H_2O_2) at a volume ratio of 7:3 for 30 minutes at 85ºC. This step generated hydroxyl (-OH) groups on the fiber surface (Fig. 1b). The fiber was then rinsed with deionized water, dried with nitrogen gas, and annealed in a vacuum oven at 110ºC for 30 minutes. During this annealing process, an approximately 0.5 cm-long section of the fiber in the middle of the 2.5 cm region was coated by a polydimethylsiloxane (PDMS) layer (prepared using the standard base: curing agent ratio of 10:1) to distinctly separate the two 1 cm-long sensing regions on the fiber (Fig. 1c).

Next, the fiber surface was modified with 3-mercaptopropyltriethoxysilane (MPTES) to introduce thiol (-SH) groups (Fig. 1d). This process involved a sol-gel deposition technique using a solution comprising 75% distilled water and 25% methanol, with a pH of nearly 4.5 adjusted using acetic acid. MPTES was added to achieve a final concentration of 2% (v/v), and the solution was allowed to react for 10 minutes to facilitate alkoxide hydrolysis and silanol formation. The fiber tip was immersed in this solution for 30 minutes, followed by rinsing with ethanol to remove any unbound silane. This step effectively eliminated excess MPTES and unreacted components from the fiber surface. Finally, the fiber was annealed at 110ºC for 30 minutes to promote condensation reactions.

The 1-cm regions of the thiol-functionalized fiber were drop coated with two different sizes of AuNPs. The AuNP solutions were prepared using the citrate reduction of hydrogen tetrachloroaurate (III) hydrate ($HAuCl_4$) following the Turkevich method [12]. When 0.01% (w/v) of $HAuCl_4$ was reduced by 1% (w/v) of sodium citrate, the average diameter of the AuNPs was around 25 nm, while reducing 0.01% of

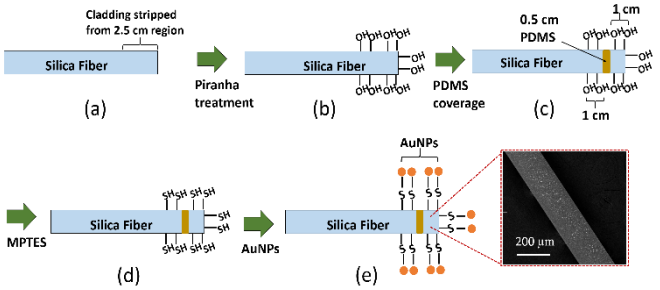

Fig. 1. The fabrication process of the dual fiber-tip LSPR sensors involves the following steps: (a) Cladding is removed from a 2.5 cm-long segment located at the tip of the silica fiber. (b) Piranha treatment forms hydroxyl functional groups on the de-cladded fiber surface. (c) PDMS coating separates two distinct sensing regions on the fiber. (d) MPTES treatment introduces thiol groups on unprotected fiber surfaces. (e) Incubating the fiber in AuNPs solution forms a fiber surface covered with AuNPs. The inset shows the SEM image of the AuNPs-coated fiber-optic LSPR sensor.

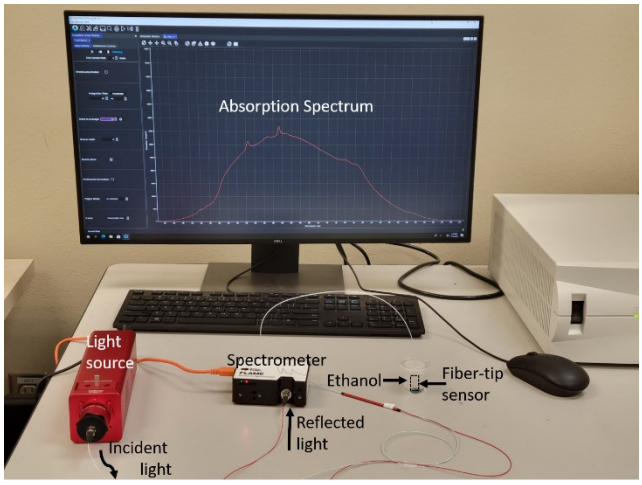

Fig. 2. (a) Experimental setup for the fiber-optic-based LSPR sensing.

$HAuCl_4$ by 0.18% of sodium citrate resulted in about 16 nm diameter of AuNPs, as was outlined in our prior work [13]. Following a 12-hour incubation in the AuNPs solutions, the fiber was rotated and subsequently drop-coated with AuNPs for another 12 hours to achieve a uniform coating of AuNPs on the cylindrical fiber surface (Fig. 1e), as confirmed by the Scanning Electron Microscopy (SEM) image in the inset highlighted with the red box. The center PDMS layer prevented the attachment of AuNPs in that region, thereby forming two distinct AuNPs-functionalized LSPR sensing regions on the same fiber. Finally, the fiber was washed with deionized water to remove any unbound nanoparticles from its surface.

B. Reflection Measurements from the LSPR Sensors

A Thorlabs fiber-coupled light source (Part # SLS201L) and an Ocean Insight spectrometer (Part # FLAME-T-VIS-NIR-ES) were used for LSPR measurements. The dual sensing regions were constructed at the fused tip of a Thorlabs 2 × 1 multimode fiber coupler (Part # TT200R5S1B), with the other ends connected to the light source and the spectrometer. The incident light traveled through the fiber via total internal reflection and illuminated the AuNPs-coated sensing regions in the fused tip. At a specific wavelength, the electrons in the AuNPs resonated with the incident light, resulting in LSPR. The spectrometer detected the reflected light from the tip area, where a peak in the absorption intensity or a dip in reflection intensity

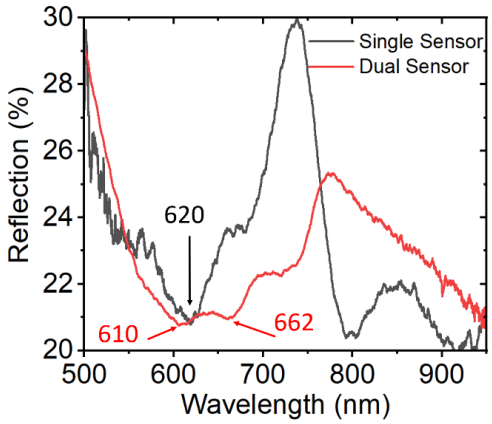

Fig. 3. A comparative analysis of reflection spectra for single versus dual sensors realized on the optical fiber.

occurred at LSPR. Due to the formation of two sensors at the fiber tip, two LSPR dips were observed in the reflection spectrum. Fig. 2 shows the optical setup for LSPR sensing and Fig. 3 shows that the reflection spectrum for a single sensor realized at the fiber tip had a single LSPR dip at 620 nm, whereas the dual sensor showed two separate LSPR dips at 610 and 662 nm. We verified that the dips resulted from LSPR by comparing the reflection spectra with those obtained from a fiber coated with agglomerated AuNPs, which lacked any LSPR dips.

III. RESULTS AND DISCUSSION

A. Sensor Calibration and Performance Metrics

The dual fiber-optic sensor was exposed to varying concentrations of ethanol (0%, 20%, 40%, 60%, 80%, and 100%) in deionized water. Fig. 4a illustrates the corresponding reflection spectra of the fiber sensor. As the concentration of ethanol (EtOH) increased, the reflection intensity decreased. This decrease can be attributed to increased scattering at the surface of the LSPR sensors due to interaction with a larger number of EtOH molecules. We observed a similar phenomenon in our previous study [14]. Additionally, the reflection spectra demonstrate two separate LSPR dips at approximately 610 and 662 nm. Fig. 4b shows the calibration curves, which were obtained by plotting the reflection intensity at the two LSPR dips (located at 610 and 662 nm) as a function of EtOH concentrations. Each calibration curve represents the relationship between the reflection intensity at the LSPR wavelength and the concentration of EtOH. These calibration curves can be used to estimate the concentration of EtOH in unknown samples by assessing the shift in LSPR intensity. Two key performance metrics of the sensor were analyzed: sensitivity and limit of detection (LOD). The calibration data were fitted with power series ($y = ax^b + c$, where a is the slope, b is the exponent, and c is the y-intercept). The sensitivity, $S_{y|x}$, was calculated by the method described in [15]:

$$S_{y|x} := \frac{dy}{dx} = abx^{b-1} \quad (1)$$

LOD was calculated using the equations (2) – (4) described in [15], [16]. First, the limit of blank (LOB) and limit of detection of the signal (yLOD) were evaluated, followed by the calculation of LOD:

$$LOB = mean\ signal\ for\ blank\ sample + 1.645 * std.dev.for\ blank\ sample \quad (2)$$

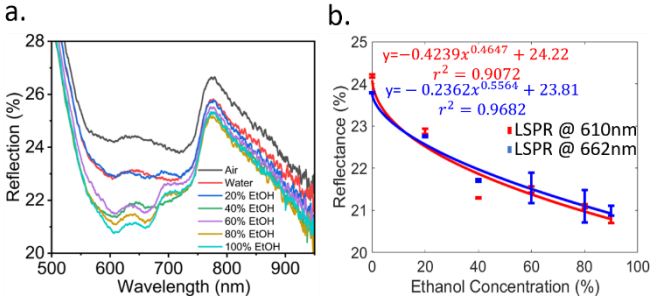

Fig. 4. (a) Reflection spectra of the fiber-optic sensor in response to varying concentrations of ethanol. (b) The calibration curves were obtained by plotting the reflection intensity at the two LSPR dips (located at 610 and 662 nm) as a function of ethanol concentrations. All measurements were repeated 3 times with the same sensor, with the error bars representing the mean and standard deviation.

$$yLOD = LOB + 1.645 * std.dev.for\ target\ at\ low\ concentration \quad (3)$$

$$LOD = \frac{yLOD - intercept\ of\ the\ calibration}{slope\ of\ the\ calibration} \quad (4)$$

The calculated sensitivity and LOD values are reported in Table 1. The signal-to-noise (SNR) ratios of the LSPR bands (21 and 26 dB) were calculated using the formula outlined in [17]. In this research, the AuNP coating was not overlaid with a selective layer to facilitate the specific adsorption of the target analyte. As a result, the variations in LSPR intensity were primarily driven by the physisorption of EtOH molecules on the AuNPs layer, causing changes in the intensity of both LSPR dips. However, we intend to expand this work in the future by applying various immobilization layers on separate AuNP-coated regions. This approach will form distinct sensing regions exhibiting selectivity towards different target analytes.

B. Sensor Performance under Varying Temperatures

The performance of the fiber-optic sensor probe was evaluated at different temperatures (25ºC, 40ºC, and 60ºC) to enable temperature correction. Fig. 5 illustrates the variations in sensor calibration in relation to the solution temperature. As the temperature of the ethanol (EtOH) solution was increased, the refractive index of the medium decreased, which in turn affected the light scattered from the sensor-solution interface. To compensate for these effects, the sensor response at a specific temperature, T, was adjusted by recalculating the intercept, slope, and exponent of the calibration curve (Fig. 4b) using equations (5) – (7) [15]. Room temperature (25ºC) was considered as the reference in these calculations:

$$intercept\ (corr.) = intercept\ (init.) * \frac{intercept_T}{intercept_{25ºC}} \quad (5)$$

$$slope\ (corr.) = slope\ (init.) * \frac{slope_T}{slope_{25ºC}} \quad (6)$$

$$exponent\ (corr.) = exponent\ (init.) * \frac{exponent_T}{exponent_{25ºC}} \quad (7)$$

Here, "corr." refers to corrected values, while "init." represents the initial values before any corrections were applied. This numerical

Table 1. Performance metrics of the sensor.

LSPR Dip	Fitted Curve	Sensitivity, $S_{y\|x}$ (reflectance%/ concentration%)	LOD (ethanol %)	SNR (dB)
610 nm	y= - 0.4239 $x^{0.4647}$ + 24.22	0.039	18.1	21
662 nm	y= - 0.2362 $x^{0.5564}$ + 23.81	0.035	18.3	26

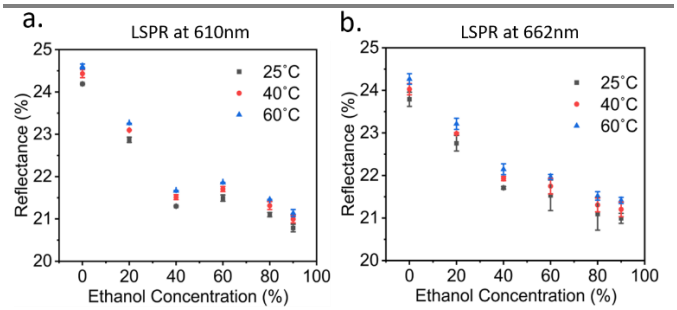

Fig. 5. Variations in the LSPR intensity at (a) 610 nm and (b) 662 nm as a function of ethanol concentrations when the temperature was also varied from 25ºC to 60ºC. The measurements were done 3 times with the same sensor. Here error bars denote mean and standard deviation.

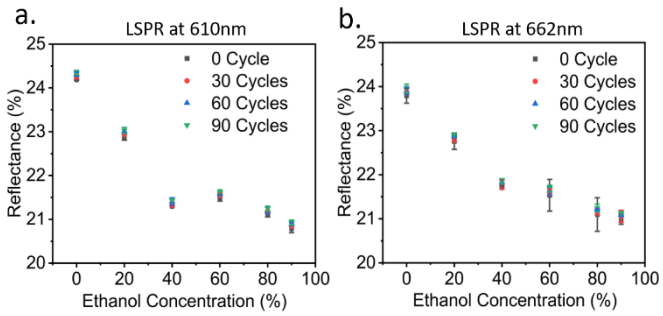

Fig. 6. Variations in the LSPR intensity at (a) 610 nm and (b) 662 nm as a function of ethanol concentrations when the fiber sensor was bent by 30, 60, and 90 cycles at an angle of 10º. The measurements were repeated 3 times. Error bars denote mean and standard deviation.

method offers a simple and more straightforward way to determine the new calibration curve at any desired temperature, eliminating the need to experimentally construct calibration plots.

C. Sensor Performance under Bending Deformations

The performance of the fiber-optic sensor was also assessed under bending deformations. The fiber was mounted on a motorized translation stage (MTS50-Z8, Thorlabs Inc., Newton, NJ, USA) and subjected to bending at an angle of 10º. After every 30, 60, and 90 cycles of bending, the calibration plot of the fiber-optic sensor was recorded for different concentrations of ethanol. As shown in Fig. 6, a negligible variation in the sensor response was observed under 10º of bending deformations. After 90 cycles of bending, the sensor response showed a coefficient of variation of less than 2.5%.

Table 2. Performance comparison of fiber-optic LSPR sensors.

Ref	Fabrication Method	Sensitivity	LOD	Multiplex
[19]	Deposition of AuNPs/SiN_x	0.0326 a.u./Brix of sucrose	0.5 Brix	No
[20]	Dip coating with AuNPs	5 x 10^{-6} a.u./pg/mL of PSA	124 fg/mL	No
[21]	Dip coating with AuNPs	0.06 μW/cm^2/ ppb of Pb^{2+}	1.2 ppb	No
This work	**Drop casting of AuNPs**	**0.039 %/% of ethanol**	**18.12 %**	**Yes**

IV. CONCLUSION AND FUTURE SCOPE

In summary, this letter reports dual fiber-optic LSPR sensors coated with gold nanoparticles and capable of exhibiting two distinct LSPR dips. Our sensor holds promise for the simultaneous measurement of two different analytes. Table 2 lists a performance comparison of our sensor with some recently reported fiber-optic LSPR sensors. It is to be noted that our work stands out from previous literature as none of the reported sensors have demonstrated the capability of multiplexing on a single fiber, making our approach distinct and novel. Our future research endeavors aim to enhance the design by integrating multiple metallic nanoparticles and selectively coated regions on the same fiber, enabling the detection of multiple analytes using a single optical fiber.

ACKNOWLEDGMENT

This work was supported in part by the National Science Foundation Award No. ECCS-2138701 and in part by the VentureWell Grant 21716-20.

REFERENCES

[1] Deschamps E, Calabrese V, Schmitz I, Hubert-Roux M, Castagnos D, Afonso C (2023), "Advances in Ultra-High-Resolution Mass Spectrometry for Pharmaceutical Analysis," *Molecules*, vol. 28, no. 5, pp. 2061, doi: 10.3390/molecules28052061.

[2] Jun S Y, Kim Y A, Lee S -J, Jung W -W, Kim H -S, Kim S -S, Kim H, Yong D, Lee K (2023), "Performance Comparison Between Fourier-Transform Infrared Spectroscopy-based IR Biotyper and Matrix-Assisted Laser Desorption/Ionization Time-of-Flight Mass Spectrometry for Strain Diversity," *Ann Lab Med*, vol. 43, no. 2, pp. 174–179, doi: 10.3343/alm.2023.43.2.174.

[3] Canales A, Jia X, Froriep U P, Koppes R A, Tringides C M, Selvidge J, Lu C, Hou C, Wei L, Fink Y, Anikeeva P (2015), "Multifunctional fibers for simultaneous optical, electrical and chemical interrogation of neural circuits in vivo," *Nat Biotechnol*, vol. 33, no. 3, Art. no. 3, doi: 10.1038/nbt.3093.

[4] Qazi R, Gomez A M, Castro D C, Zou Z, Sim J Y, Xiong Y, Abdo J, Kim C Y, Anderson A, Lohner F, Byun S -H, Lee B C, Jang K -I, Xiao J, Bruchas M R, Jeong J -W (2019), "Wireless optofluidic brain probes for chronic neuropharmacology and photostimulation," *Nat Biomed Eng*, vol. 3, no. 8, Art. no. 8, doi: 10.1038/s41551-019-0432-1.

[5] Calcerrada M, García-Ruiz C, González-Herráez M (2015), "Chemical and biochemical sensing applications of microstructured optical fiber-based systems," *Laser & Photonics Reviews*, vol. 9, no. 6, pp. 604–627, doi: 10.1002/lpor.201500045.

[6] Yang X, Gong C, Zhang C, Wang Y, Yan G -F, Wei L, Chen Y -C, Rao Y -J, Gong Y (2022), "Fiber Optofluidic Microlasers: Structures, Characteristics, and Applications," *Laser & Photonics Reviews*, vol. 16, no. 1, p. 2100171, doi: 10.1002/lpor.202100171.

[7] Blue R, Uttamchandani D (2016), "Recent advances in optical fiber devices for microfluidics integration," *Journal of Biophotonics*, vol. 9, no. 1–2, pp. 13–25, doi: 10.1002/jbio.201500170.

[8] Tabassum S, Nayemuzzaman S K, Kala M, Mishra A K, Mishra S K (2022), "Metasurfaces for Sensing Applications: Gas, Bio and Chemical," *Sensors*, vol. 22, no. 18, Art. no. 18, doi: 10.3390/s22186896.

[9] Desmet C, Vindas K, Meza R A, Garrigue P, Voci S, Sojic N, Maziz A, Courson R, Malaquin L, Leichle T, Buhot A, Roupioz Y, Leroy L, Engel E (2020), "Multiplexed Remote SPR Detection of Biological Interactions through Optical Fiber Bundles," *Sensors*, vol. 20, no. 2, Art. no. 2, doi: 10.3390/s20020511.

[10] Poeggel S, Duraibabu D, Tosi D, Leen G, Lewis E, McGrath D, Fusco F, Sannino S, Lupoli L, Ippolito J, Mirone V (2015), "Differential in vivo urodynamic measurement in a single thin catheter based on two optical fiber pressure sensors," *J Biomed Opt*, vol. 20, no. 3, p. 037005, doi: 10.1117/1.JBO.20.3.037005.

[11] Srivastava S K, Arora V, Sapra S, Gupta B D (2012), "Localized Surface Plasmon Resonance-Based Fiber Optic U-Shaped Biosensor for the Detection of Blood Glucose," *Plasmonics*, vol. 7, pp. 261–268, doi: 10.1007/s11468-011-9302-8.

[12] Turkevich J, Stevenson P C, Hillier J (1951), "A study of the nucleation and growth processes in the synthesis of colloidal gold," *Discuss. Faraday Soc.*, vol. 11, no. 0, pp. 55–75, doi: 10.1039/DF9511100055.

[13] Noushin T, Hossain N I, Tabassum S (2022), "IoT-Enabled Integrated Smart Wound Sensor for Multiplexed Monitoring of Inflammatory Biomarkers at the Wound Site," *Frontiers in Nanotechnology*, vol. 4, doi: 10.3389/fnano.2022.851041.

[14] Tabassum S, Aryal S (2022), "Real-time quantification of CD63 with anti-CD63 functionalized plasmonic fiber optic probe," in *Optical Fibers and Sensors for Medical Diagnostics, Treatment and Environmental Applications XXII*, SPIE, pp. 18–22. doi: 10.1117/12.2604375.

[15] Hossain N I, Tabassum S (2023), "A hybrid multifunctional physicochemical sensor suite for continuous monitoring of crop health," *Sci Rep*, vol. 13, no. 1, Art. no. 1, doi: 10.1038/s41598-023-37041-z.

[16] Armbruster D A, Pry T (2008), "Limit of blank, limit of detection and limit of quantitation," *Clin Biochem Rev*, vol. 29 Suppl 1, no. Suppl 1, pp. S49-52.

[17] Rodrigues M S, Pereira R M S, Vasilevskiy M I, Borges J, Vaz F (2020), "NANOPTICS: In-depth analysis of NANomaterials for OPTICal localized surface plasmon resonance Sensing," *SoftwareX*, vol. 12, pp. 100522, doi: 10.1016/j.softx.2020.100522.